

## Fault strength in thin-skinned tectonic wedges across the smectite-illite transition: constrains from friction experiments and critical tapers.

Telemaco Tesei<sup>1</sup>, Brice Lacroix<sup>2</sup>, and Cristiano Collettini<sup>3</sup>

<sup>1</sup>*Istituto Nazionale di Geofisica e Vulcanologia, Via di Vigna Murata 605, 00143, Rome, Italy*

<sup>2</sup>*Department of Earth and Environmental Sciences, University of Michigan, Ann Arbor, Michigan 48109-1005, USA*

<sup>3</sup>*Department of Earth Sciences, University La Sapienza, Piazzale Aldo Moro, Rome, Italy*

### FAULT ZONE ARCHITECTURE AND FAULT ROCK DETAILS

Fault rock samples were carefully sampled from the shear zones associated to the Monte Coscerno thrust, MCT (Northern Apennines) and Monte Perdido thrust, MPT (Southern Pyrenees), schematic cross-sections to highlight their structural position along the décollement are reported in Figure DR2, and further details of regional compressional tectonics, fault geometry, fault rocks and deformation mechanisms have been extensively described in Lacroix et al., 2011, 2012, 2013 and by Tesei et al., 2013, 2014 for the MCT and MPT, respectively. Lithology, fault zone architecture and deformation mechanisms of the MCT and MPT fault zones show remarkable analogies with other exhumed detachment faults documented throughout the world (e.g. Byrne and Fisher 1987; Byrne 1990; Labaume et al., 1997; Vannucchi et al., 2008; Festa et al., 2010; Meneghini et al., 2012; Chester et al., 2013; Laurich et al., 2014; Hansberry et al., 2014).

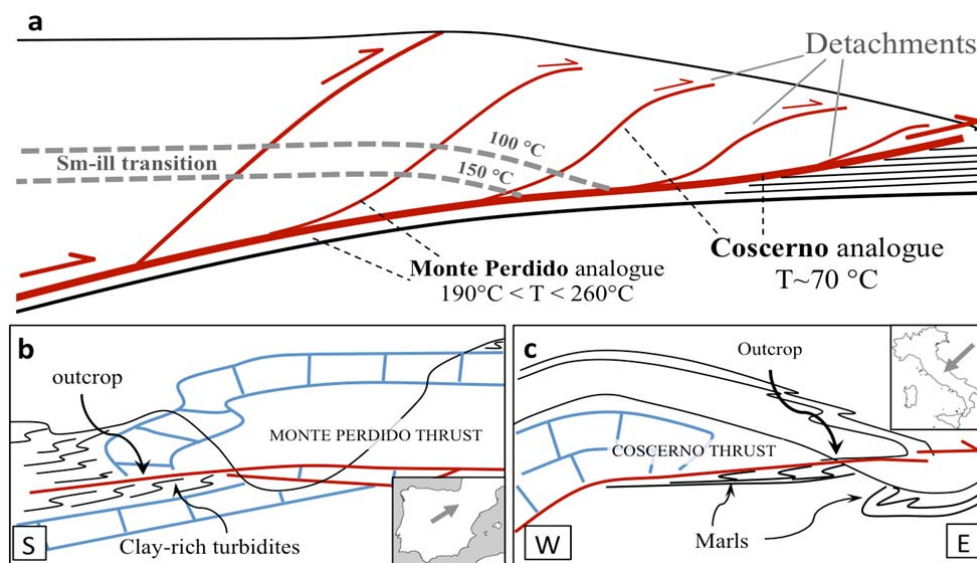


Figure DR1. Schematic cross sections of the b) Monte Perdido thrust and c) Monte Coscerno Thrust.

**Monte Coscerno thrust (MCT) fault:** sample locality: Usigni-Fonte Colle di Mezzo 42.715240, 12.895936

**Monte Perdido thrust (MPT) fault:** sample locality: Torla 42.644527, -0.109302

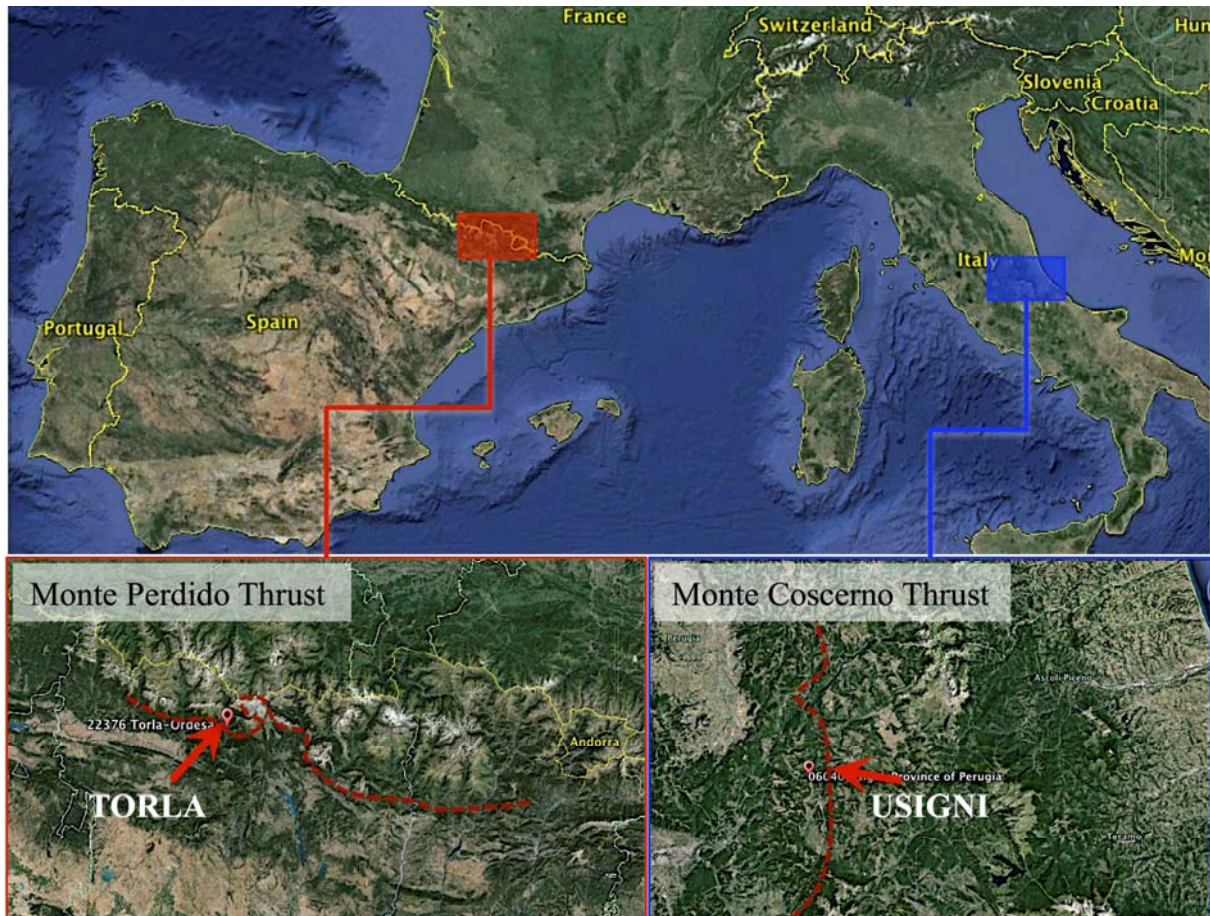


Figure DR2. Location of the Monte Perdido Thrust and Monte Coscerno Thrust faults. (Modified from Lacroix et al., 2011; Tesei et al. 2013).

### Monte Coscerno Thrust

The MCT thrust in the Usigni sample location has about 10 km of Displacement (Tesei et al., 2014) and it juxtaposes competent Cretaceous carbonates (the Scaglia Bianca/Rossa Fm) on top of Eocene clay-rich marls Marls (Scaglia Variegata/Scaglia Cinerea Fm).

The MCT fault zone is highly affected by lithological heterogeneities because such large thrusts involve a carbonatic passive margin sequence, which may produce complex mechanical and seismic behaviour (e.g. see Tesei et al., 2014). However, when incompetent lithologies such as marls are involved in the deformation, the typical structure of the fault zone consists of a thick shear zone (tens to hundreds of meters thick) that extends both in the hangingwall and the footwall blocks (Figure DR3). This shear zone is characterized by clay-rich, foliated S-CC' rocks that is analogue

to faults developed in trench-fill sediments typical of subduction channels or the front of other accretionary wedges (e.g. Byrne et al., 1990; Vannucchi et al., 2008; Ogata et al., 2012).

These fault zones accommodate significant strain with pervasive shearing along the foliation due to pressure-solution creep and frictional sliding along clays (e.g. Tesei et al., 2013; Viti et al., 2014), generally with limited cataclastic deformation. Foliated fault rocks (e.g. Figure DR4) surround and cross-cut localization features at different scales (from tens of meters to the cm scale) that accommodate larger slip in the fault zone (histograms in Figure DR3). Such localization features are typically anastomosing and discontinuous, suggesting a continuous interplay with the clay-rich foliation (i.e. synchronous sliding). Tectonic mixing, bedding disruption and boudinage are often associated to these localization features; moreover the abundance of synthetic shears suggests that slip is energetically favored within the thick shear zones (Tesei et al., 2013).

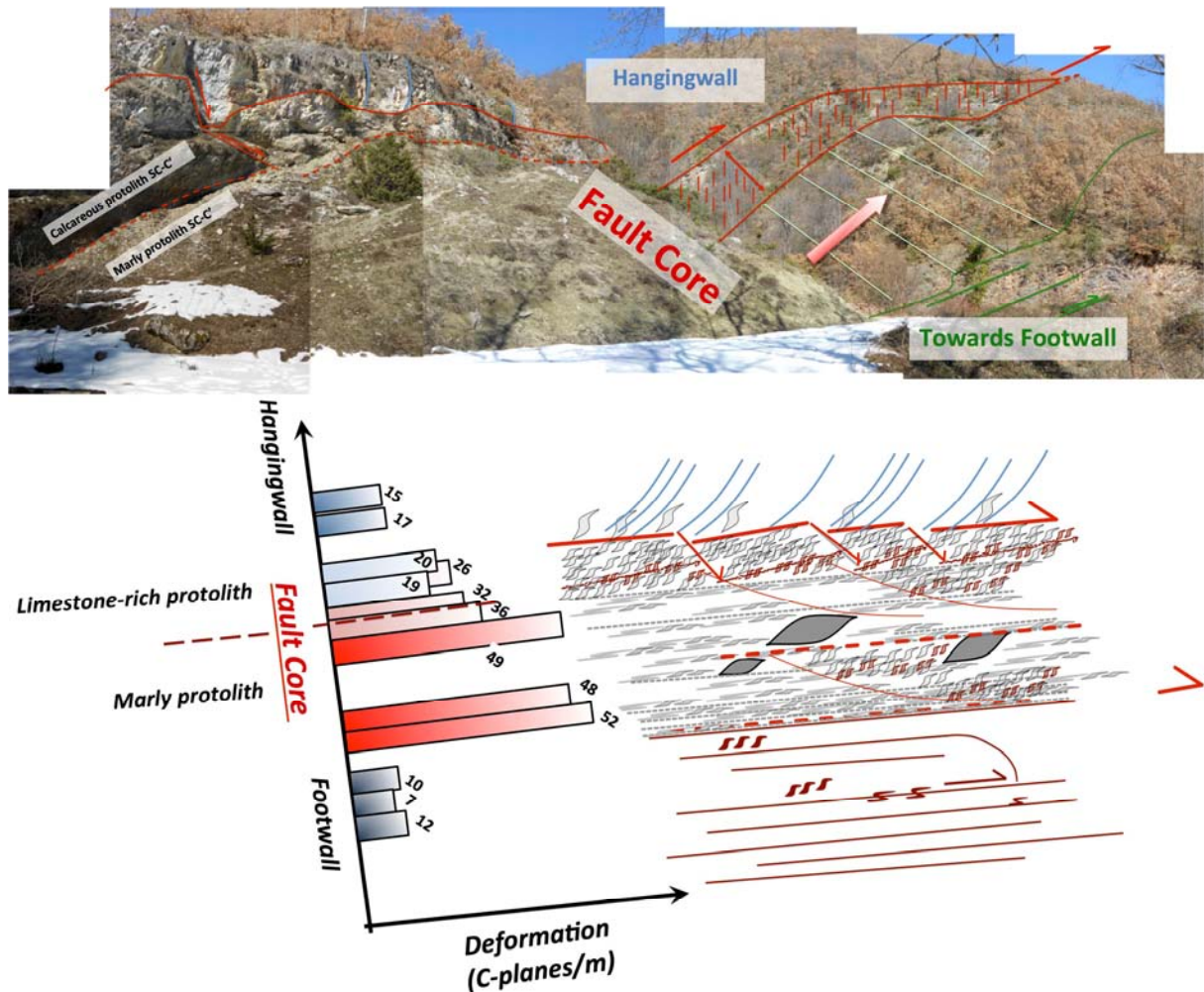
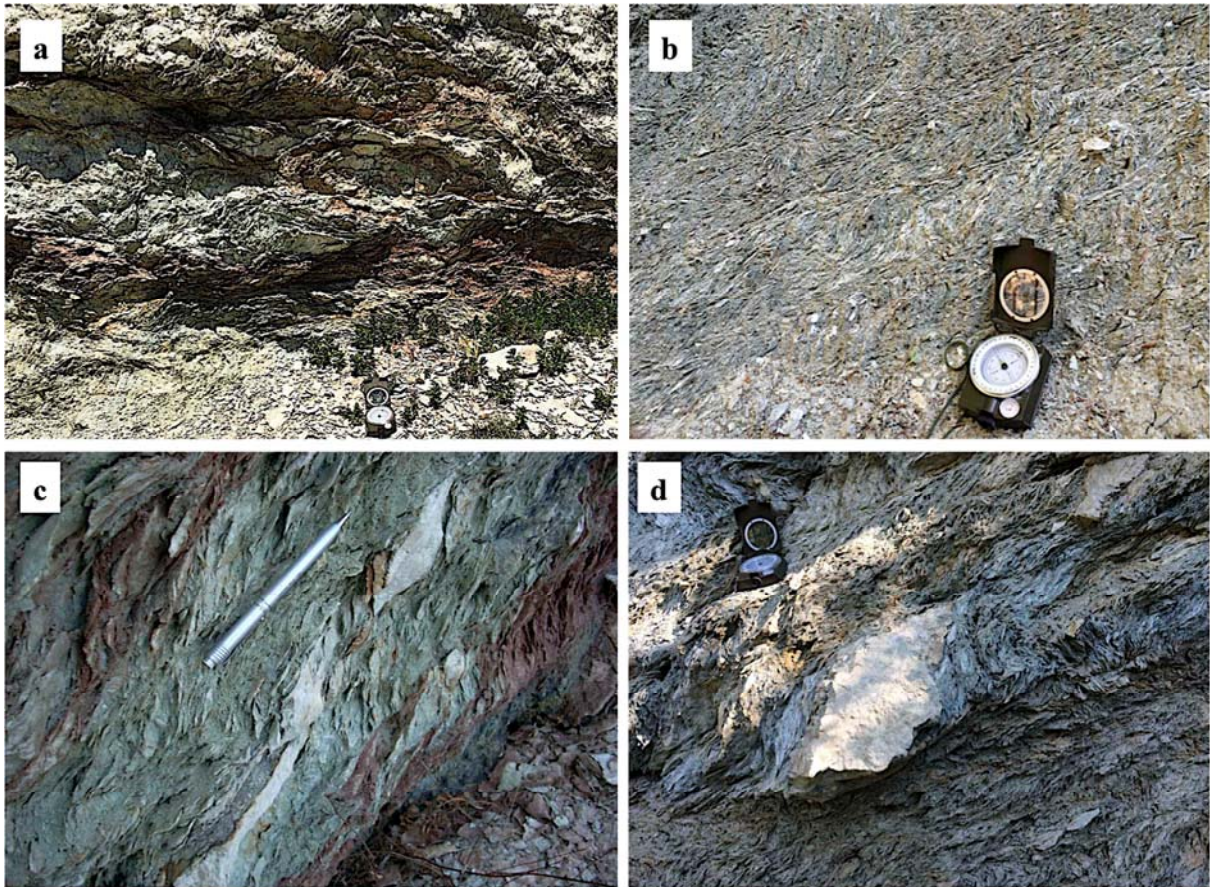


Figure DR3. Large-scale fault zone architecture of the MCT: marl protolith (grey), marly limestone protolith (pink), localization features (red). Localization occurs at different scales and is characterized by a closely spaced foliation with respect to the surrounding fault rocks. The histogram on the left highlights the number of C planes in one meter of fault zone thickness.



**Figure DR4.** a) tectonic mixing of marls (grey), marly limestones (red) and pelagic limestones (white, top of the figure) along localized anastomosing shear zones. b) S-CC' tectonites in Marls. c) S-CC' tectonites in marly limestone. d) Boudinaged blocks of calcarenite immersed in ductile S-CC' tectonites. This is the location of MCT samples used in friction experiments.

Fault rocks for the experiments have been sampled close to localization features (e.g. Figure DR4d) and within the most foliated domains in order to capture the natural fabric within lab-scale samples. Because of such localization features, we interpret the frictional sliding along the foliation as an upper bound of the fault strength.

### Monte Perdido Thrust

The Monte Perdido thrust fault has about 6 km displacement (Séguret 1972). In the studied outcrop the fault zone juxtaposes competent Paleocene limestone on the top of Eocene turbidite sequences (Hecho Group).

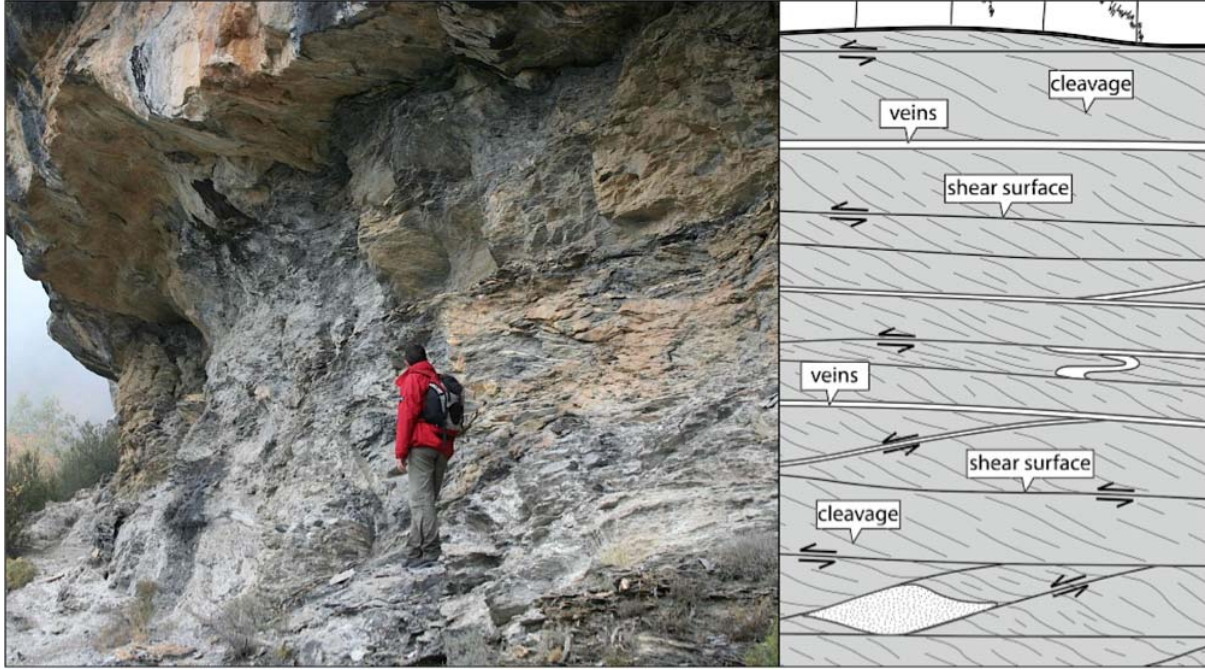


**Figure DR5. Monte Perdido thrust fault zone.**

The fault core zone is about 6 m thick and consists of an interval of intensely deformed clay-bearing rocks (Figure DR5). The fault zone accommodates significant strain along shear surfaces and cleavage due to pressure-solution creep and frictional sliding along clays (Lacroix et al. 2012; 2013) without any evidence of cataclastic deformation. Such localization features are typically anastomosing and define C-C'-S structures. Decametric to centimetric deformed competent lenses incorporated from hanging wall and footwall blocks are commonly embedded within the cleavage. calcite and quartz rich shear veins along the shear planes are abundant.

Locally, the fault zone is strongly deformed, with a more intense cleavage suggesting that these levels accommodated higher strain. These levels are marked by the presence of chlorite coating shear surfaces. The deformation here is strictly frictional and it is completely accommodated by shearing along shear surfaces and foliation (Lacroix et al., 2013).

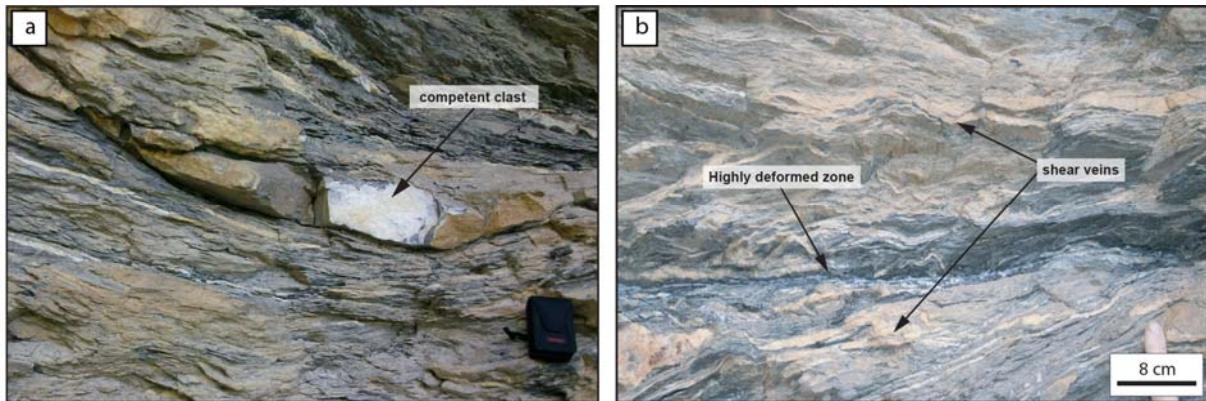
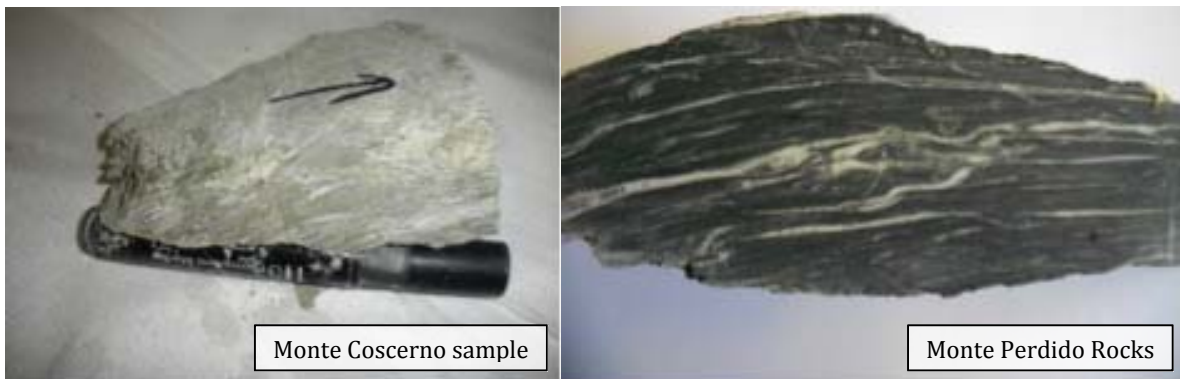


Figure DR6. a) Boudinaged sandstone block within the MPT core. b) Highly deformed horizon sampled for friction experiments.

## INTACT FAULT ROCK COMPOSITION



### Monte Coscerno Thrust rocks

The MCT rocks used in this study are essentially binary mixtures of calcite and smectite with negligible amounts of oxides (quartz, goethite) and Apatite (Viti et al., 2014). Smectite clays in the fault zone are highly variable due to the anisotropic nature of the fault rock foliation and lithologies involved, ranging from ~20 to 50% of the total volume. In natural rocks, slip is localized within almost purely clay horizons that outline the scaly fabric (Tesei et al., 2013).

To estimate the composition of MCT rocks used in the experiments, we analyzed powders produced from wafers used in friction tests. XRD patterns (Performed at the Siena University, courtesy of Prof. Cecilia Viti) show abundance of calcite and Ca-montmorillonite with traces of quartz (Figure DR7).

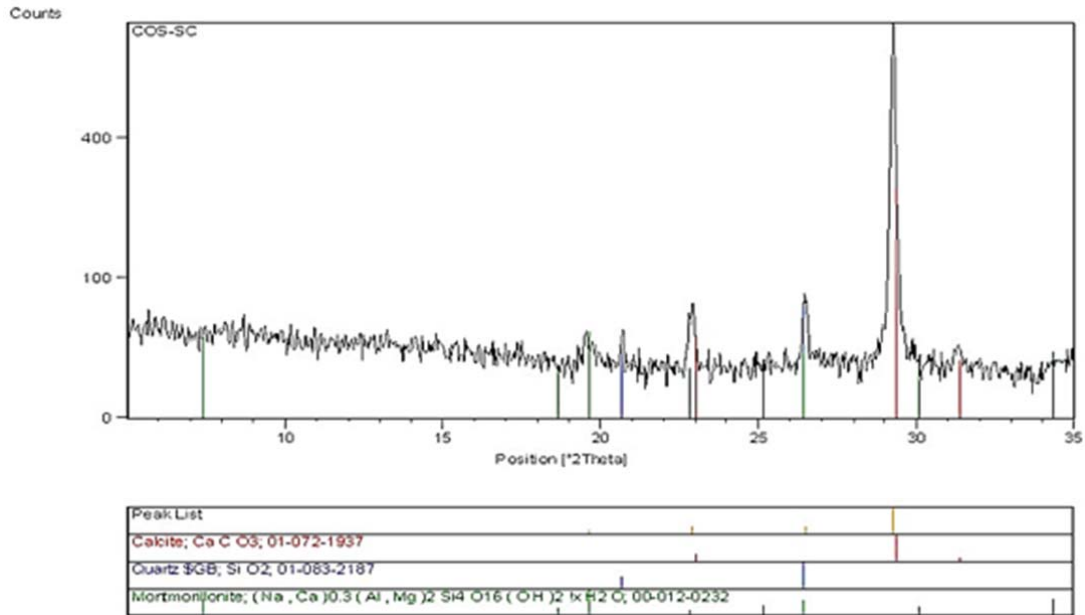


Figure DR7. XRD diffraction from MCT rocks highlights the presence of calcite and smectitic clays.

Then, we performed Thermogravimetric analysis to estimate calcite amounts via CO<sub>2</sub> CaO departure. These analysis show that the remaining material (decomposed clay fraction), after complete decarbonation, represents ~35% of the sample.

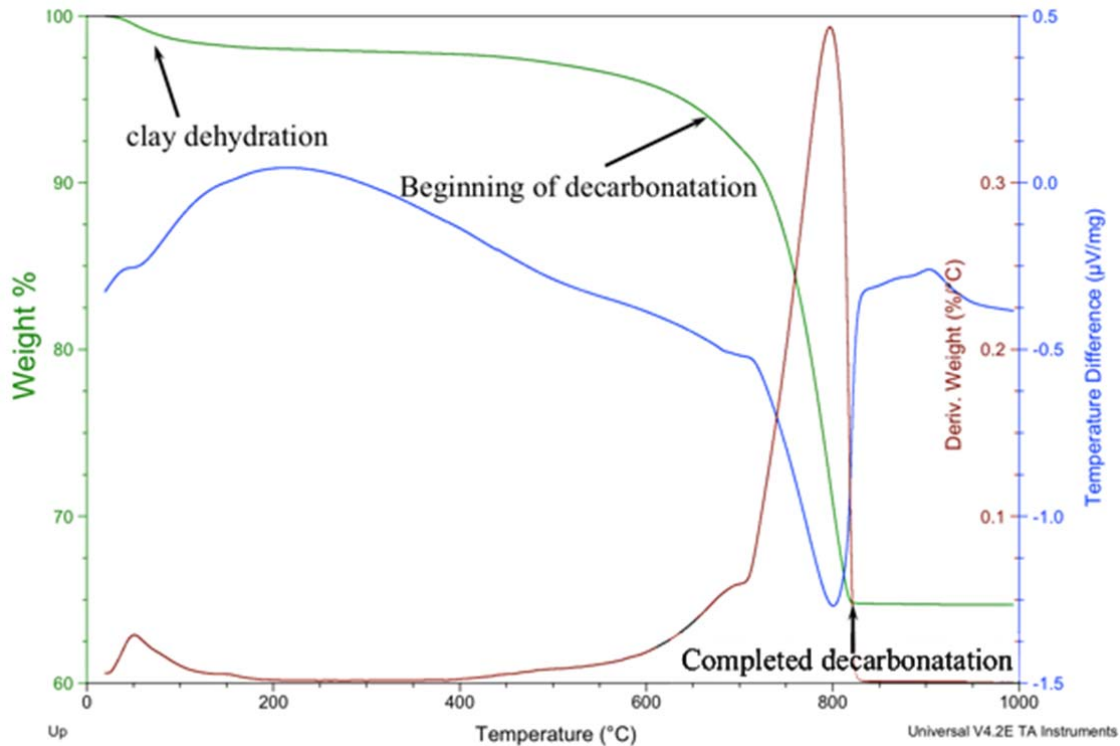


Figure DR8. Results of thermogravimetric analysis on MCT rocks.

Monte Perdido Thrust rocks

XRD diffraction performed on the MPT samples shows the presence of 4 principal mineralogical phases: illite, chlorite, quartz and calcite (Figure DR9).

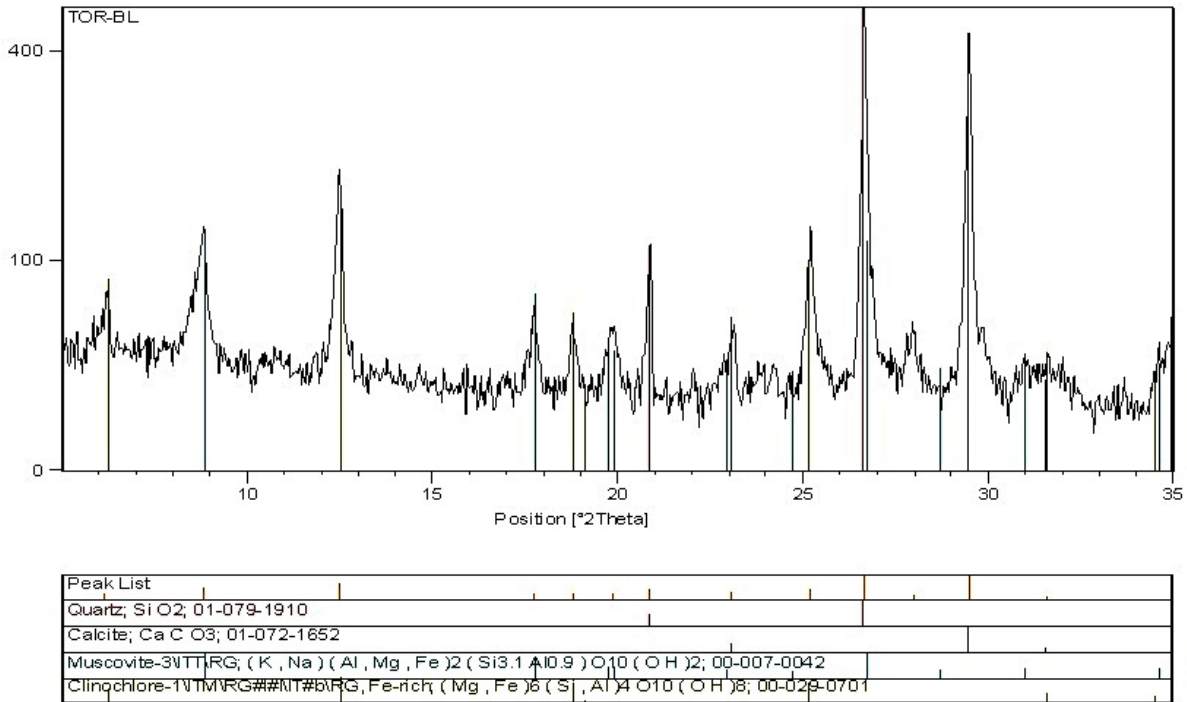
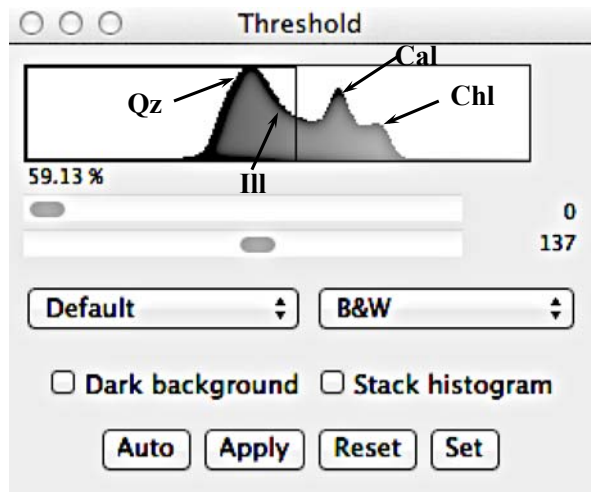


Figure DR9. XRD diffraction for MCT rocks. Highlighted the presence of calcite and quartz, illite and chlorite clays.

To quantitatively constrain the volume of clay phases (illite and chlorite) we performed image analysis on a suite of 4 SEM pictures of the foliation (pre-experimental, undeformed samples). We used the software ImageJ with the Smoothing and Thresholding tools. In back-scattered SEM microscopy the intensity of the color (in grayscale) is directly proportional to the reflection and thus to atomic weight. On this basis, intensity color peaks can be separated and thresholded areas roughly correspond to each single mineral phase (example in figure here on the right).

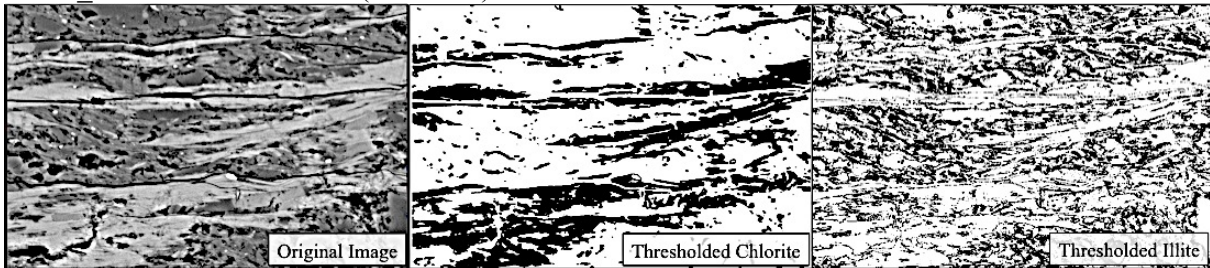
The procedure followed for the image analysis was the following: 1) Crop out labels 2) Smooth if the picture is pixelated.3) Threshold each different phase in a separate picture (Ill, Chl, Qz, Cal, after removing holes in the section). 4) Compute pixel percentage of each phase, normalized to the area without holes.



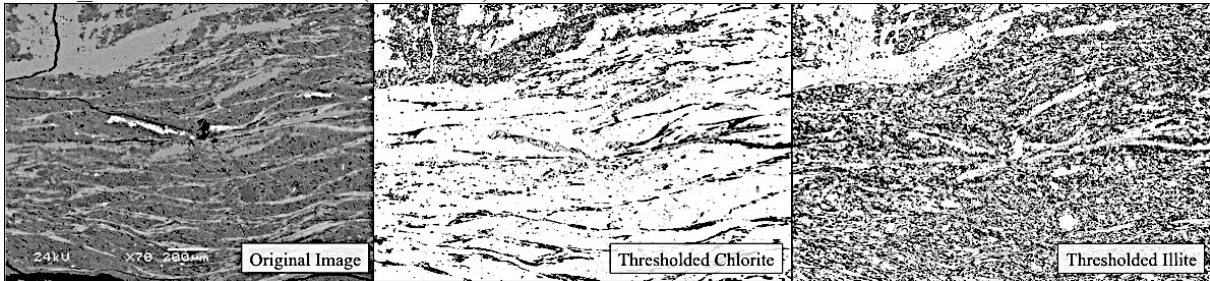
## RESULTS

Note: the long side of each figure is ~800  $\mu\text{m}$  long.

Tor21\_24 Chl=27% Ill=25% (Tot. 52%)



Tor21\_27 Chl=13% Ill=29% (Tot. 42%)



Tor 21\_29 Chl=11% Ill=39% (Tot. 50%)



Tor21\_35 Chl=14% Ill=42% (Tot. 56%)



These results suggest that MPT samples used in friction experiments contained about 50% of total phyllosilicates.

## EXPERIMENTAL SETUP AND DETAILS

**Table DR1** summarizes all the tests carried out in the present work and their relative experimental conditions.

Exp. Name	Fault / Fabric	Normal Stress (MPa)	Type of experiment
i075	Monte Perdido / intact wafers	20-39	VS + SHS*
i079	Monte Perdido / intact wafers	75	only sliding
i133	Monte Perdido / intact wafers	10-53	VS + SHS
i077	Monte Perdido / intact wafers	20	only sliding**
i109	Monte Perdido / intact wafers	30	only sliding**
i078	Monte Perdido / intact wafers	20	only sliding (dry)**
i104	Monte Perdido / intact wafers	15	only sliding**
i113	Monte Perdido / intact wafers	30	only sliding**
i070	Monte Perdido / powders	20-39	VS + SHS
i071	Monte Perdido / powders	10-53	VS + SHS
i074	Monte Perdido / powders	75-100	only sliding
i026	Coscerno / intact wafers	10	VS + SHS*
i100	Coscerno / intact wafers	53	VS + SHS*
i135	Coscerno / intact wafers	20-39	VS + SHS*
i136	Coscerno / intact wafers	75	only sliding
i163	Coscerno / intact wafers	30	only sliding
i134	Coscerno / powders	10	VS + SHS*
i152	Coscerno / powders	53	VS + SHS*
i153	Coscerno / powders	75	only sliding
i157	Coscerno / powders	20-39	VS + SHS*
*Velocity stepping, VS, tests ( $v= 1-3-10-30-100 \mu\text{m/s}$ ) and slide-hold-slide, SHS, tests (1-3-10-30-100-300-1000 s hold time).			
**Sliding tests designed to evaluate the pseudo-cohesion of the Monte Perdido foliated rocks (see text for further details).			

Samples of S-CC' tectonites were hand-cut via a precision diamond rotary blade into rectangular wafers 50x50x~12 mm to fit the sample holders. Then, they were maintained under 100% humidity environment for several days before the experiments, in order to adsorb water and ensure better saturation. Throughout the experiments, the samples were kept under water submersion.

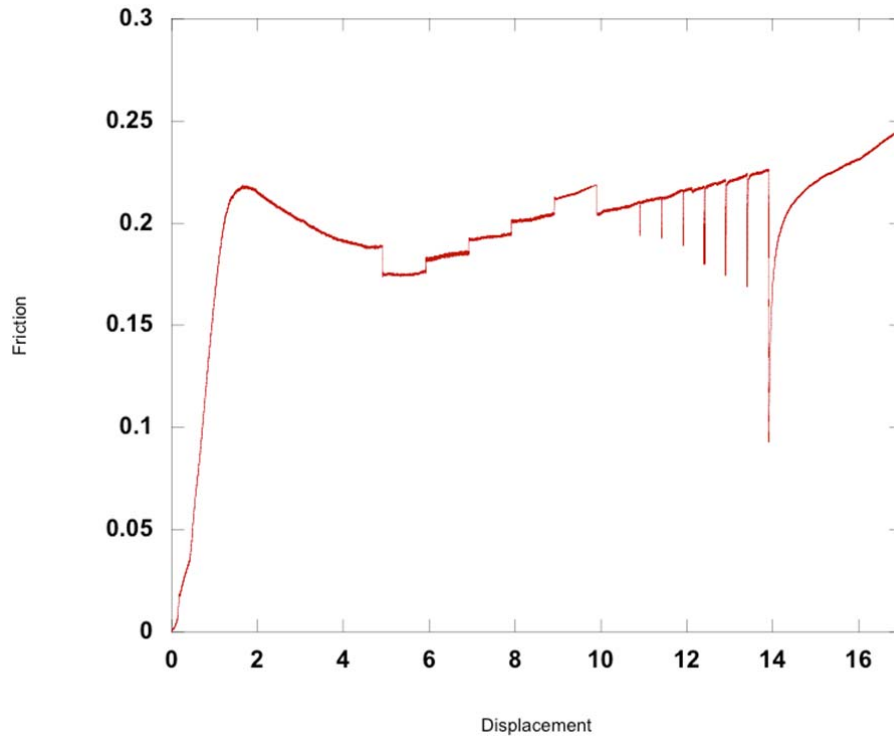


Figure DR10. Typical friction experiments with an intact MPT rock, under 10 and 30 MPa of normal stress. Friction increases during the elastic loading up to a peak and then evolves to steady state. Then the velocity stepping sequence and slide-hold-slide tests are started. The last part of the curve represents shearing at a different normal stress (30 MPa). Last hardening trend is interpreted to be caused by the final consumption of the foliation and the beginning of deformation by frictional sliding and/or cataclasis of calcite.

Before shearing, we waited for the complete saturation of the samples under 1 kN of applied normal force. Then, normal force was gradually increased up to the desired normal load, subsequently maintained throughout the experiment. Each shearing experiment (e.g. Figure DR10) consisted of a “run-in” shear carried out at constant loading velocity  $10\mu\text{m/s}$  that lasted several mm until “steady” state friction or constant slope of the friction curve was attained. Subsequently, the samples were subjected to an increase in normal load and then shearing started again and/or computer-controlled sequences of velocity steps (1 to  $300\mu\text{m/s}$  shearing velocity) and slide-hold-slide (hold periods up to 3000 s) were initiated.

Figure DR11 illustrates some experimental curves, demonstrating significant difference in friction between intact fault rocks and their respective powders.

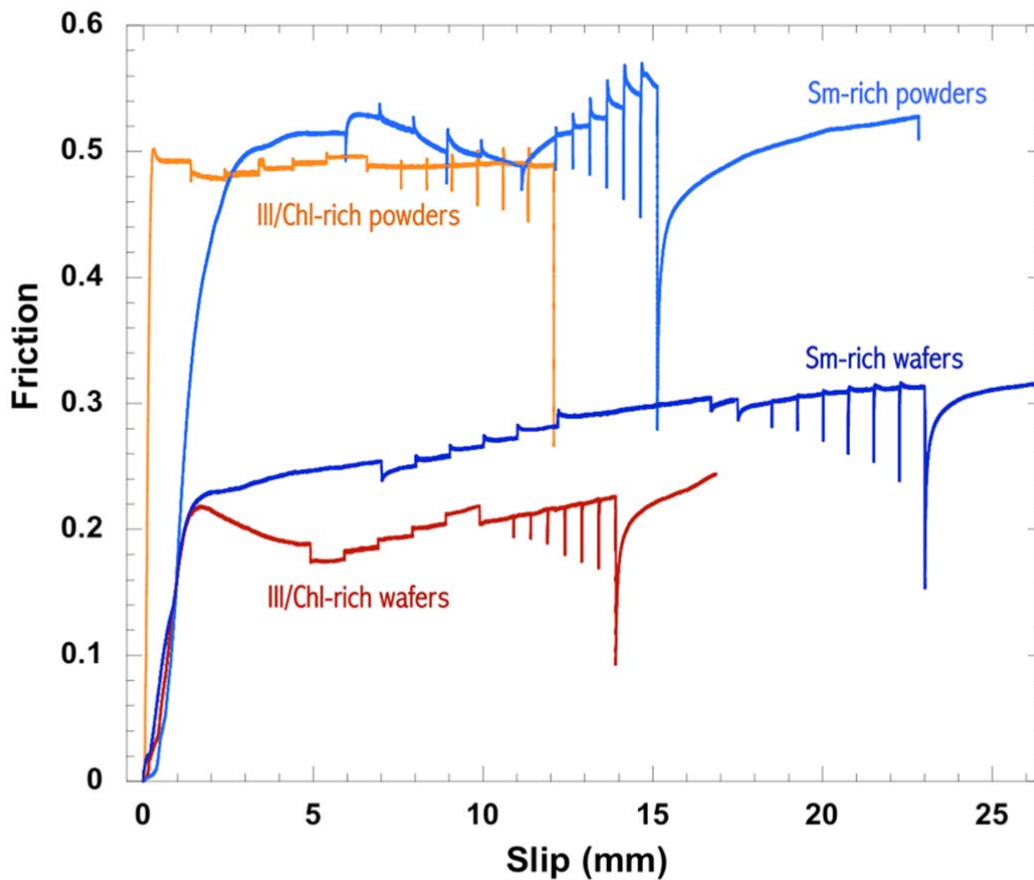


Figure DR11. Typical friction curves of powders (upper part) and intact foliated fault rocks. (Blue and red curves represent friction at two different applied normal stresses).

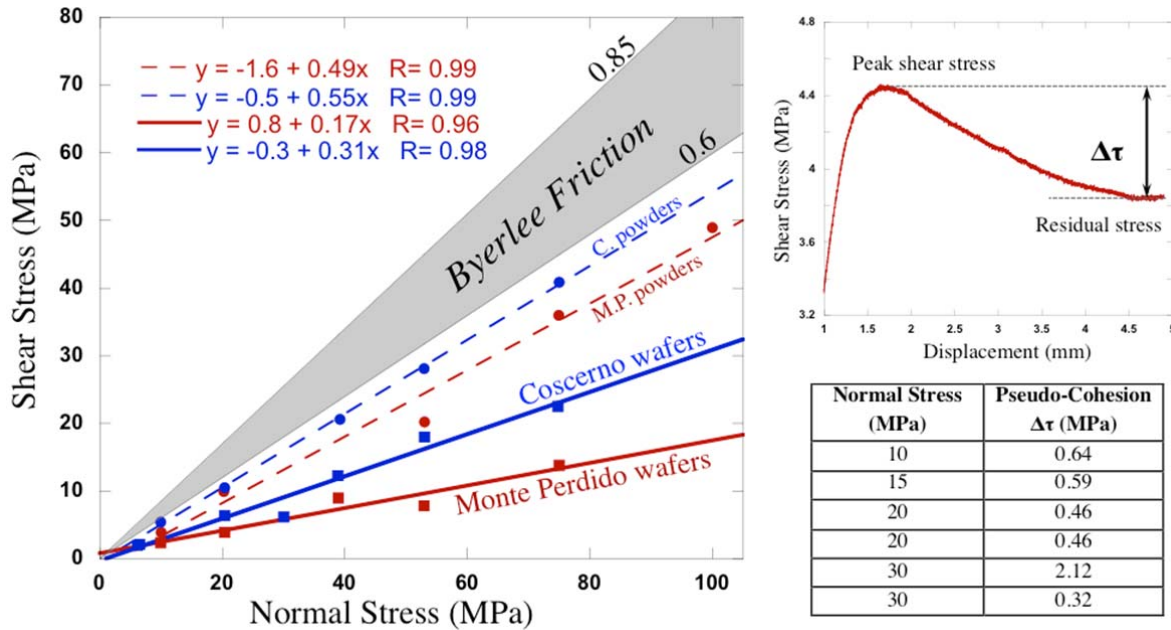


Figure DR12. a) Mohr-Coulomb envelope and linear regression equations b) Shear stress evolution from peak to steady state for a MPT wafer, regarded as “pseudocoheion” of an intact rock c) table showing pseudocoheion for all 6 experiments in which peak-to-steady state strength degradation has been observed.

In Figure DR12a are shown the linear fit equations not reported in Figure 2a in the main text.

High correlation coefficients demonstrate fairly uniform mechanical properties of each set of samples. Cohesion, defined as the intercept with the Y axis of the linear trend, is negligible since it is within the experimental error range. If we consider the cohesion as the breakdown from peak to “steady-state” shear strength, this occurs only in 6 out of 13 wafer experiments and only in MPT rocks. This strength breakdown is generally observed to be lower than 0.7 MPa.

### PRE- versus POST-EXPERIMENTAL OBSERVATIONS

In fault rock wafers, the constant measurement of low friction coefficients (Figure DR11) is attributed to i) highly standardized experimental procedure ii) sliding along the interconnected phyllosilicate horizons, despite of the significant sample-scale anisotropy of hard minerals (i.e. only the foliation strength and connectivity influence the friction coefficient).

In fact in both pre- and post- experimental samples, shear veins, and clasts of the original lithology are rather undeformed, witnessing frictional sliding along the foliation. Here we show the example of 3 MCT rock specimens (Figure DR13), one naturally deformed, i.e. sampled from the fault zone, one compacted under 30 MPa of normal stress but not sheared, and one sheared for ~20 mm under 30 MPa of applied normal stress. In all cases intact rock clasts are intact within a well-interconnected shear foliation indicating that during shearing most of the deformation is accommodated by frictional sliding along the clays and cataclasis of stronger granular grains such as calcite and quartz is not occurring.

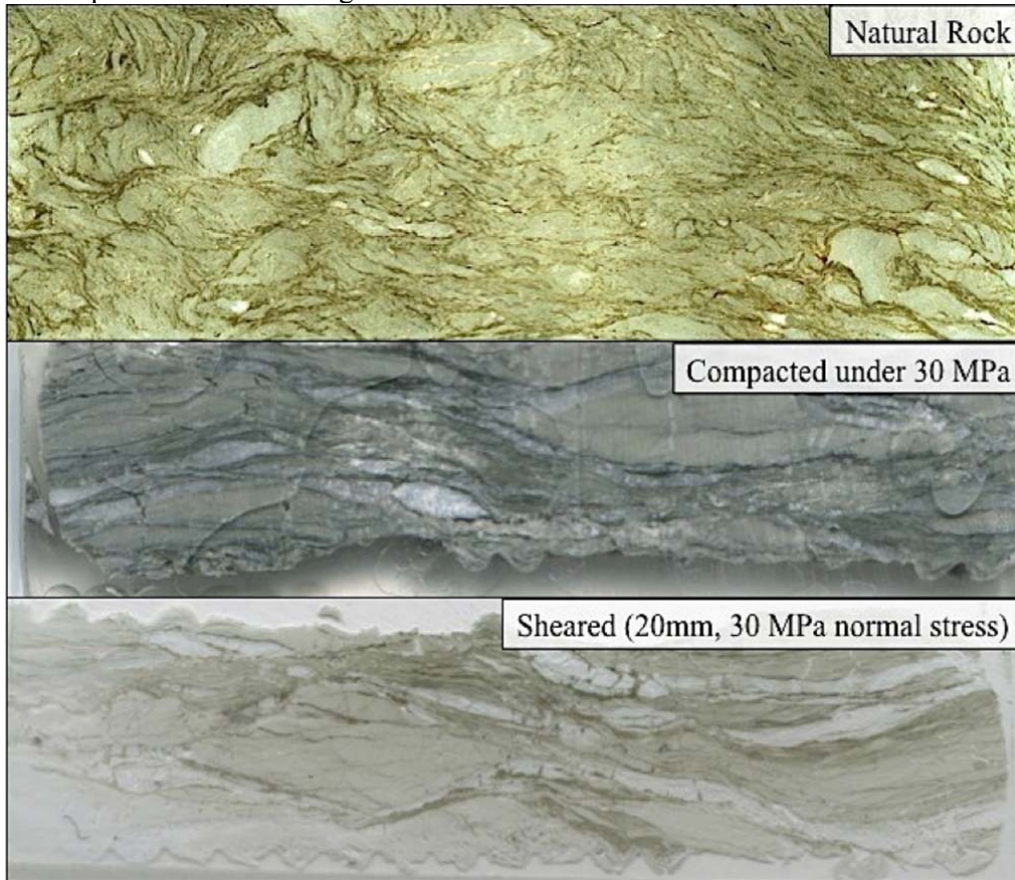
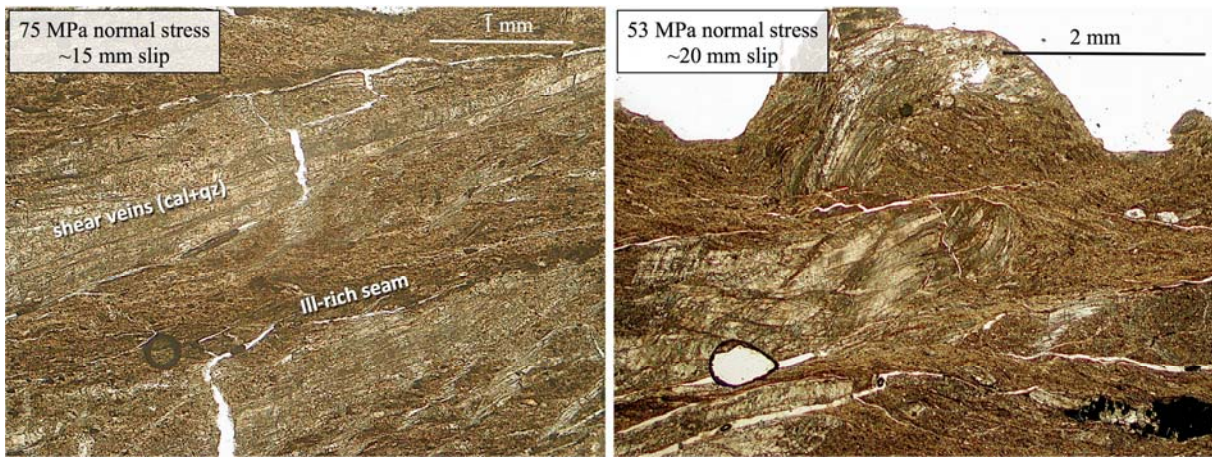


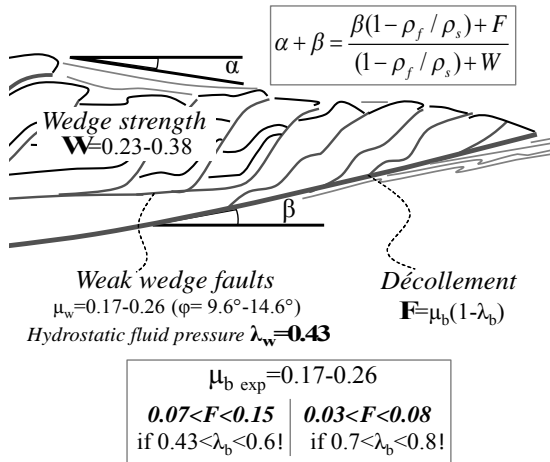
Figure DR13. a) natural MCT sample. b) MCT sample compacted under 30 MPa of normal stress (not sheared). c) Post-experimental sample (i163) in which the foliation accommodated ~20 mm slip. In all samples calcite veins and pockets of original rocks are globally undeformed. Length of all images is ~5mm.

In the following Figure DR14 we present examples of MPT (ill/chl- rich) post-experimental samples with intact clasts and interconnected foliation. Here again frictional sliding along phyllosilicates accommodates most of the deformation.



**Figure DR14. a) Post experimental microstructure of sample i079, MPT wafers sheared under 75 MP normal stress. b) microstructures of experiment i133. 53 MPa normal stress. In both samples natural fibrous calcite veins lie intact within the foliation**

## REFERENCES FOR TAPER ANGLES OF ACCRETIONARY PRISMS



Wedge	$\alpha$	$\beta$	F (W=0.23)	F (W=0.38)	Reference
Barbados	3°	2°	0.05	0.06	Dahlen, 1990
Cascadia	1.1°	2.8°	0.03	0.04	Lallemand et al., 1994
Hikurangi (South)	1°	3°	0.03	0.04	Fagereng, 2011
Makran	2°	2.5°	0.04	0.05	Smith et al., 2012
Nankai (East)	1.5°	2.6°	0.03	0.04	Saffer & Bekins, 2002
Sumatra (South)	2°	3°	0.04	0.05	Kopp & Kukowski, 2003
Taiwan	2°	2.7°	0.04	0.05	Carena et al., 2002
<b>Low tapers</b>			<b>0.03 &lt; F &lt; 0.06</b>		
Aleutians	3.4°	3.9°	0.06	0.08	Lallemand et al., 1994
Chile (South)	5°	6°	0.09	0.12	Von Huene & Ranero, 2003
Costa Rica	3.5°	6°	0.07	0.10	Von Huene & Ranero, 2003
Java	3.1°	6°	0.07	0.09	Davis et al., 1983
Kurile (South)	1.3°	9.7°	0.06	0.09	Lallemand et al., 1994
Kermadec	3.7°	6.8°	0.08	0.11	Lallemand et al., 1994
Hikurangi (North)	3.5°	7.5°	0.08	0.11	Fagereng, 2011
Nankai (West)	5°	3°	0.08	0.10	Saffer & Bekins, 2002
Peru	6.5°	4°	0.11	0.14	Von Huene & Ranero, 2003
<b>Moderate tapers</b>			<b>0.06 &lt; F &lt; 0.14</b>		

Critical taper model parameters (from text Figure 3) and references of wedge geometry.

Carena, S., Suppe, J., and Kao, H., 2002, Active detachment of Taiwan illuminated by small earthquakes and its control of first-order topography: *Geology*, v. 30, p. 935–938, doi:10.1130/0091-7613(2002)030<0935:ADOTIB>2.0.CO;2.

Dahlen, F.A., 1990, Critical taper model of fold-and-thrust belts and accretionary wedges: *Annual Review of Earth and Planetary Sciences*, v. 18, p. 55–99, doi:10.1146/annurev.earth.18.050190.000415.

Davis, D., Suppe, J., and Dahlen, F.A., 1983, Mechanics of fold-and-thrust belts and accretionary wedges: *Journal of Geophysical Research*, v. 88, B2, p. 1153–1172, doi:10.1029/JB088iB02p01153.

Fagereng, A., 2011, Wedge geometry, mechanical strength and interseismic coupling of the Hikurangi subduction thrust, New Zealand: *Tectonophysics*, v. 507, p. 26–30, doi:10.1016/j.tecto.2011.05.004.

Kopp, H., and Kukowski, N., 2003, Backstop geometry and accretionary mechanics of the Sunda margin: *Tectonics*, v. 22, doi:10.1029/2002TC001420.

Lallemand, S.E., Schnürle, P., and Malavieille, J., 1994, Coulomb theory applied to accretionary and nonaccretionary wedges: Possible causes for tectonic erosion and/or frontal accretion: *Journal of Geophysical Research*, v. 99, B6, p. 12033–12055, doi:10.1029/94JB00124.

Saffer, D.M., and Bekins, B.A., 2002, Hydrologic controls on the morphology and mechanics of accretionary wedges: *Geology*, v. 30, p. 271–274, doi:10.1130/0091-7613(2002)030<0271:HCOTMA>2.0.CO;2.

Smith, G., McNeill, L., Henstock, T.J., and Bull, J., 2012, The structure and fault activity of the Makran accretionary prism: *Journal of Geophysical Research*, v. 117, p. B07407, doi:10.1029/2012JB009312.

Von Huene, R., and Ranero, C.R., 2003, Subduction erosion and basal friction along the sediment-starved convergent margin off Antofagasta, Chile: *Journal of Geophysical Research*, v. 108, B2, doi:10.1029/2001JB001569.